Gut-derived circulating bacterial vesicles reduce systemic carbapenem exposure and sustain extraintestinal infections

Guoxiu Xiang[1,6], Jialin Huang[2,3,6], Junying Zhu[1,6], Ziyu Yang[1], Qianqian Gao[1], Tianchi Chen[1], Yan Song[1], Xilong Zhang[1], Yiwei Zhu[4], Chen Wang[1], Juanxiu Qin[1], Haomin Zhang[1], Hua Wang[1]✉, Min Li[1,5]✉, Zhen Shen[1]✉

[1]Department of Laboratory Medicine, Renji Hospital, School of Medicine, Shanghai Jiao Tong University, Shanghai, China

[2]Department of Neurosurgery, Renji Hospital, Shanghai Jiao Tong University School of Medicine, Shanghai, China

[3]Shanghai Institute of Head Trauma, Shanghai, China

[4]Department of Critical Care Medicine, Renji Hospital, School of Medicine, Shanghai Jiao Tong University, Shanghai, China

[5]School of Nursing, Shanghai Jiao Tong University, Shanghai, China

[6]These authors contributed equally: Guoxiu Xiang, Junying Zhu, Ziyu Yang.

✉Corresponding authors:

zhenshen@shsmu.edu.cn (Zhen Shen)

rjlimin@shsmu.edu.cn (Min Li)

renjijywh@shsmu.edu.cn (Hua Wang)

Extended data Table 1. Clinical characteristics of patients with persistent and non-persistent carbapenem-susceptible *Enterobacterales* infections.

Clinical characteristics	Persistent infection (n=262)	Control (n=766)	*P* value
Demographics			
Age, median (IQR), y	64.6±15.1	66.6±13.9	0.483
Male sex, n(%)	168 (64.1)	454 (59.3)	0.188
Length of hospital stay (days)	45.2±10.6	36.1±9.7	0.062
Co-morbidities, n(%)			
COPD	54 (20.6)	174 (22.7)	0.547
Chronic liver disease	74 (28.2)	230 (30.0)	0.638
Chronic renal disease	82 (31.3)	191 (24.9)	0.052
Solid organ transplant	40 (15.3)	122 (15.9)	0.845
Solid cancer	34 (13.0)	86 (11.2)	0.437
Infection sites, n(%)			
Respiratory tract	90 (34.4)	317 (41.4)	**0.048**
Intra-abdominal	33 (12.6)	110 (14.4)	0.535
Multi-site infection	109 (41.6)	117 (15.3)	**<0.001**
Invasive procedures, n(%)			
Mechanical ventilation	68 (26.0)	96 (12.5)	**<0.001**
Abdominal drains	31 (11.8)	71 (9.3)	0.233
Central venous catheter	38 (14.5)	67 (8.7)	**0.013**
Urinary catheter	22 (8.4)	56 (7.3)	0.589
Chemotherapy/radiotherapy in the last 3 months, n(%)	26 (10.3)	68 (8.9)	0.620
Enterobacterales species in cases, n(%)			
K. pneumoniae	98 (37.4)	314 (41.0)	0.343
E. coli	63 (24.0)	176 (23.0)	0.735
E. cloacae	40 (15.3)	109 (14.2)	0.685
Others	59 (22.5)	163 (21.3)	0.665
ESBLs-producing *Enterobacterales*	135 (51.5)	345 (45.0)	0.073
Antibiotics, n(%)			
BLBLIs	69 (26.3)	236 (30.8)	0.183
Carbapenems	65 (24.8)	172 (22.5)	0.445
Cephalosporins	45 (17.2)	129 (16.8)	0.924
Fluoroquinolones	35 (13.4)	93 (12.1)	0.590
Aminoglycosides	24 (9.2)	86 (11.2)	0.418
Combination therapy	35 (13.4)	152 (19.8)	**0.020**
Fecal CRE colonization, n(%)			
CREC	38 (14.5)	14 (1.8)	**<0.001**
CRKP	9 (3.4)	33 (4.3)	0.557

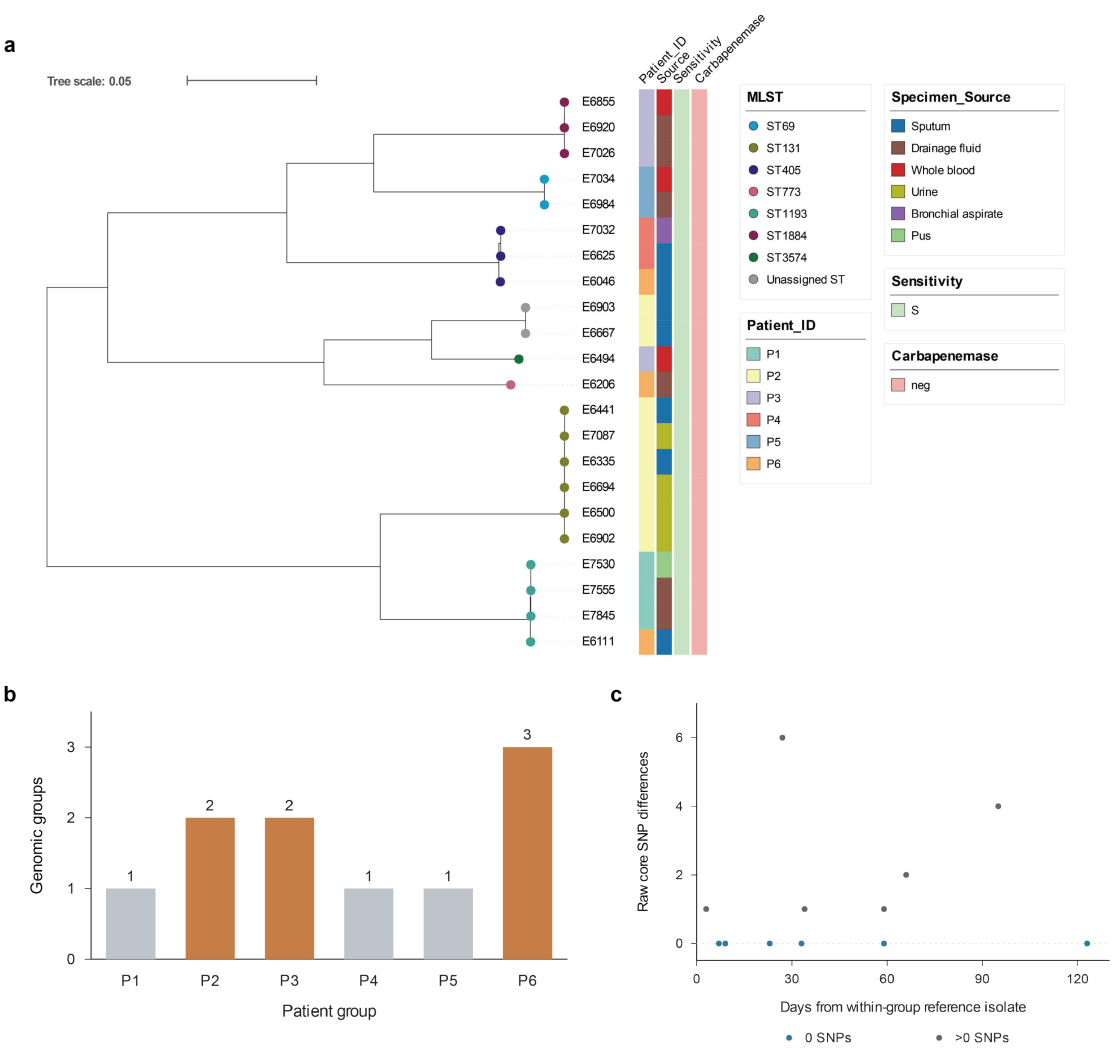
Data are presented as mean ± standard deviation (SD), median (interquartile range [IQR]), or number of patients (%). *P* values were calculated using the unpaired two-sided Student's t-test,

Mann-Whitney test, $\chi 2$ test, or Fisher's exact test, as appropriate. COPD, chronic obstructive pulmonary disease; ESBLs, extended-spectrum β-lactamase; BLBLIs, β-lactam/β-lactamase inhibitors; CREC, carbapenem-resistant *Escherichia coli*; CRKP, carbapenem-resistant *Klebsiella pneumoniae*.

Extended data Table 2. Univariate and multivariate analysis of risk factors for persistent extraintestinal infection.

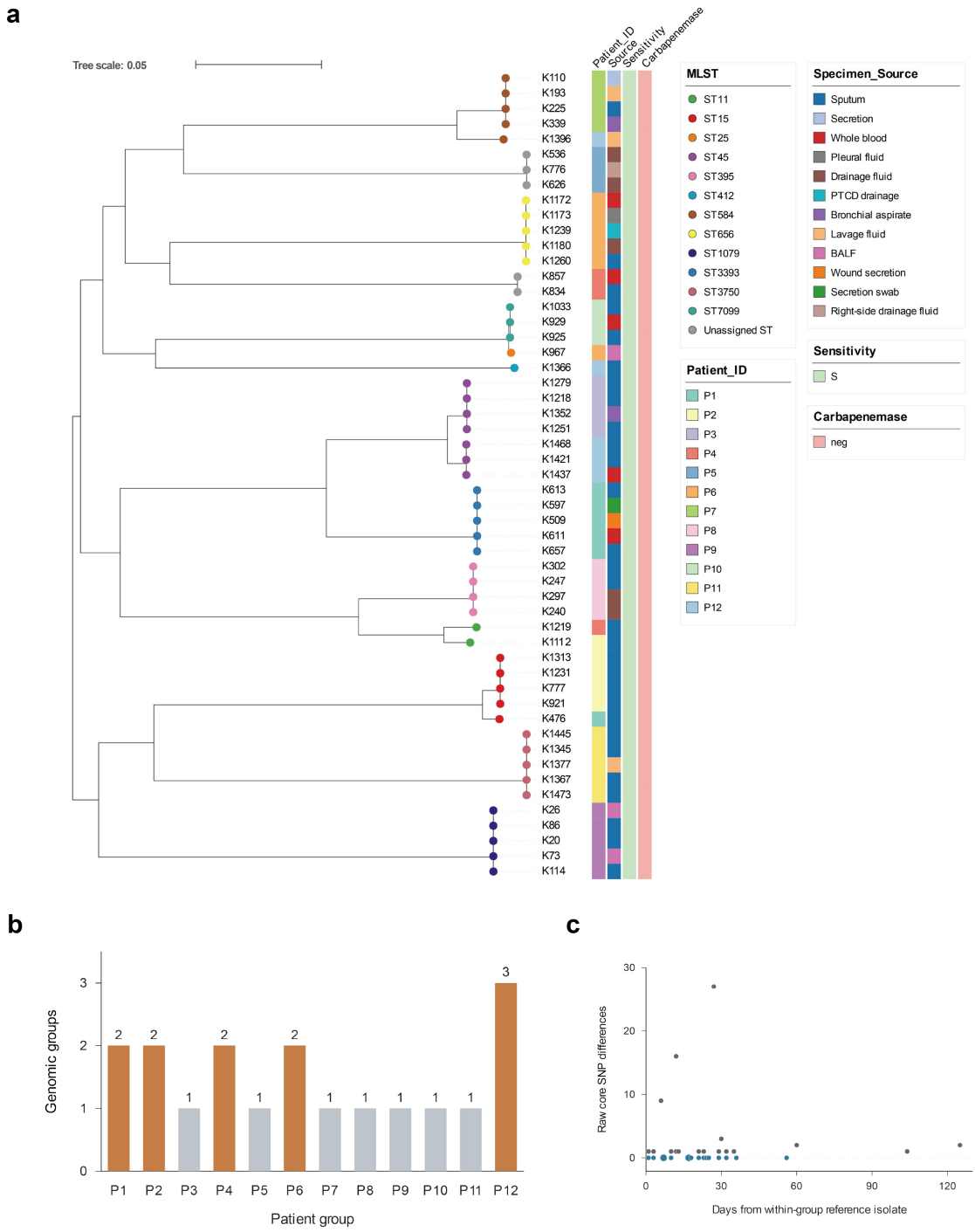
Clinical characteristics	OR (95% CI)	*P* value	OR (95% CI)	*P* value
Demographics				
Age, median (IQR), y	0.894 (0.723-1.351)	0.324		
Male sex, n (%)	1.228 (0.918-1.643)	0.166		
Length of hospital stay (days)	1.358 (1.026-1.653)	0.072		
Co-morbidities, n(%)				
COPD	0.883 (0.626-1.246)	0.479		
Chronic liver disease	0.917 (0.673-1.251)	0.585		
Chronic renal disease	1.371 (1.008-1.866)	**0.045**	1.388 (0.988-1.949)	0.059
Solid organ transplant	0.951 (0.645-1.402)	0.800		
Solid cancer	1.179 (0.771-1.803)	0.447		
Infection sites, n(%)				
Respiratory tract	0.741 (0.553-0.993)	**0.045**	0.751 (0.545-1.036)	0.081
Intra-abdominal	0.859 (0.566-1.304)	0.476		
Multi-site infection	3.952 (2.885-5.414)	**<0.001**	4.154 (2.975-5.801)	**<0.001**
Invasive procedures, n(%)				
Mechanical ventilation	2.446 (1.725-3.469)	**<0.001**	2.326 (1.581-3.422)	**<0.001**
Abdominal drains	1.314 (0.840-2.055)	0.232		
Central venous catheter	1.770 (1.156-2.709)	**0.009**	1.986 (1.245-3.168)	**0.004**
Urinary catheter	1.162 (0.695-1.944)	0.567		
Chemotherapy/radiotherapy in the last 3 months, n(%)	1.131 (0.703-1.819)	0.612		
Enterobacterales species in cases, n(%)				
K. pneumoniae	0.860 (0.644-1.148)	0.307		
E. coli	1.061 (0.763-1.476)	0.724		
E. cloacae	1.086 (0.733-1.609)	0.681		
Others	1.075 (0.767-1.507)	0.674		
ESBL-producing *Enterobacterales*	1.297 (0.979-1.718)	0.070		
Antibiotics, n(%)				
BLBLIs	0.803 (0.586-1.099)	0.172		
Carbapenems	1.139 (0.821-1.581)	0.435		
Cephalosporins	1.024 (0.705-1.486)	0.901		
Fluoroquinolones	1.116 (0.735-1.693)	0.606		
Aminoglycosides	0.797 (0.495-1.283)	0.351		
Combination therapy	0.623 (0.418-0.927)	**0.020**	0.652 (0.425-1.001)	0.051
Fecal CRE colonization, n(%)				
CREC	8.833 (4.691-16.631)	**<0.001**	8.719 (4.446-17.099)	**<0.001**
CRKP	0.791 (0.431-1.455)	0.518		

The table displays odds ratios (OR) with corresponding 95% confidence intervals (CI). Statistical analysis was performed using univariate and multivariate logistic regression models to identify independent clinical predictors of persistent infection. COPD, chronic obstructive pulmonary disease; ESBLs, extended-spectrum β-lactamase; BLBLIs, β-lactam/β-lactamase inhibitors; CREC, carbapenem-resistant *Escherichia coli*; CRKP, carbapenem-resistant *Klebsiella pneumoniae*.



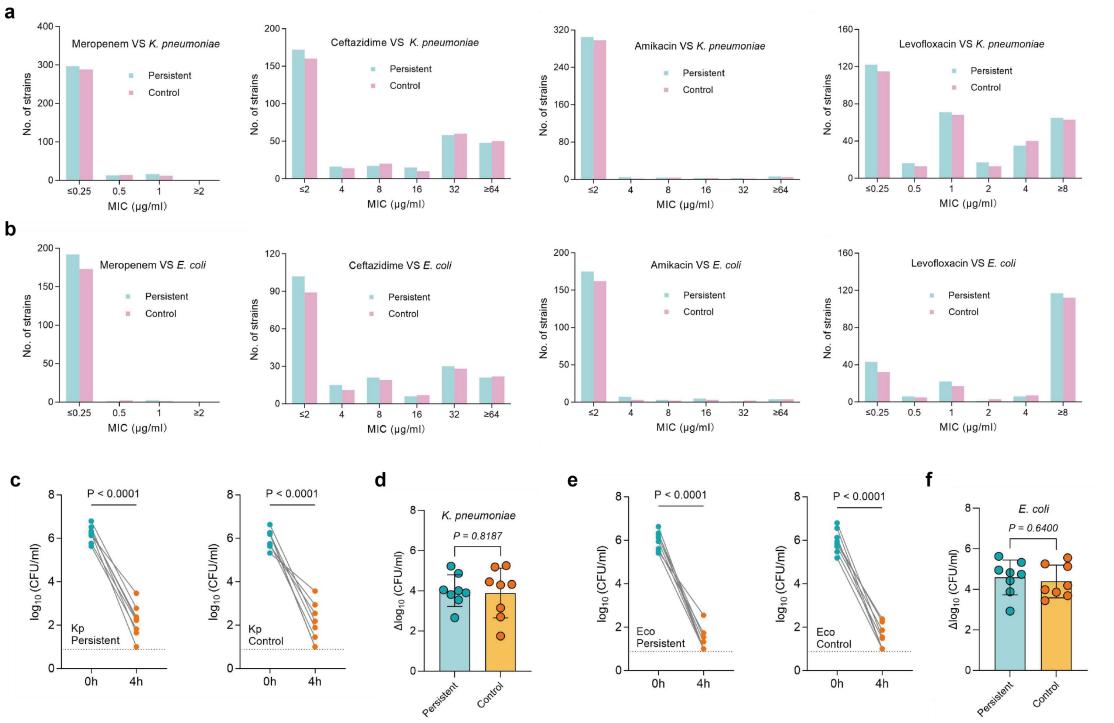
Extended Data Fig. 1. Genomic characterization of longitudinal *Escherichia coli* isolates from persistent extraintestinal infections. **a**, Core-genome phylogenetic tree of carbapenem-susceptible *Escherichia coli* isolates collected longitudinally from 6 randomly selected patients (P1-P6) with persistent infections. The annotations display the multi-locus sequence type (MLST), patient ID, clinical specimen source, carbapenem susceptibility, and carbapenemase status (all negative). **b**, Number of distinct genomic groups identified per patient over the infection course, illustrating either the persistence of a single genomic group or clonal replacement. Genomic groups were defined by the sequence types of the *E. coli* strains isolated from each

patient. **c**, Pairwise raw core-genome single-nucleotide polymorphism (SNP) differences among longitudinal isolates within the same genomic group, plotted against the days from the initial within-group reference isolate. The data show a maximum accumulation of 6 SNPs over a 120-day period.

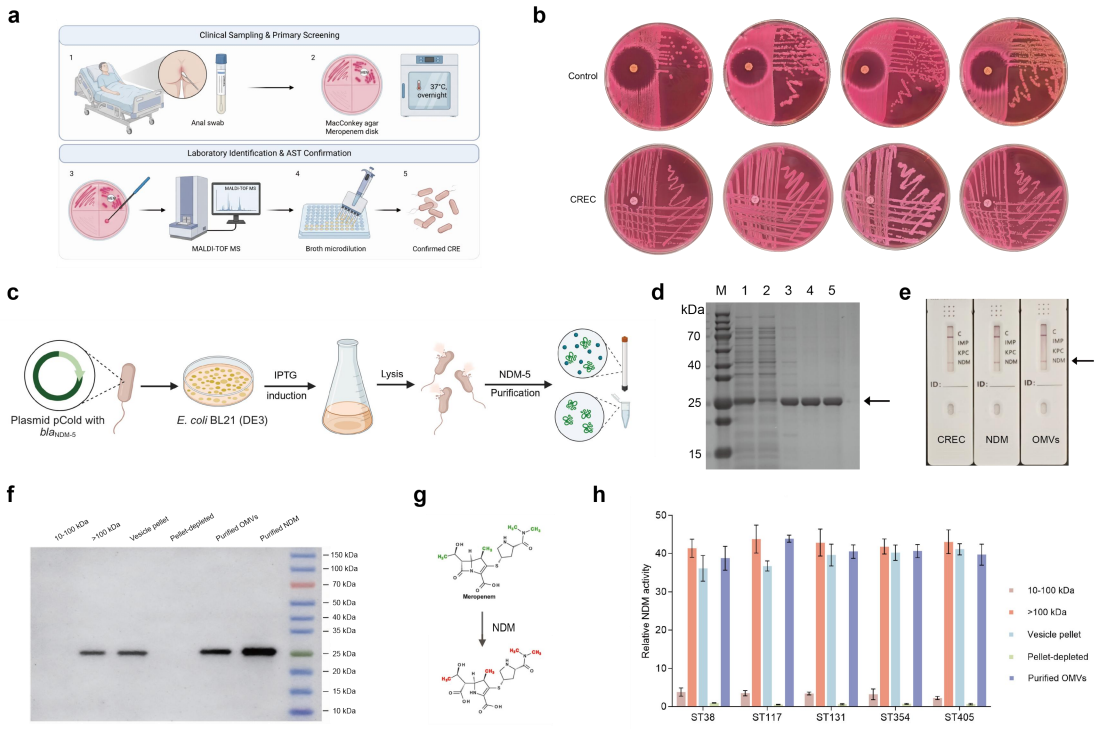


Extended Data Fig. 2. Genomic characterization of longitudinal *Klebsiella pneumoniae* isolates from persistent extraintestinal infections. **a**, Core-genome phylogenetic tree of carbapenem-susceptible *K. pneumoniae* isolates collected longitudinally from 12 randomly selected patients (P1-P12) with persistent infections.

Annotations display the multi-locus sequence type (MLST), patient ID, clinical specimen source, carbapenem susceptibility, and carbapenemase status (all negative). **b**, Number of distinct genomic groups identified per patient over the infection course, illustrating either the persistence of a single genomic group or clonal replacement. Genomic groups were defined by the sequence types of the *K. pneumoniae* strains isolated from each patient. **c**, Pairwise raw core-genome single-nucleotide polymorphism (SNP) differences among longitudinal isolates within the same genomic group, plotted against the days from the initial within-group reference isolate. The data demonstrate minimal SNP accumulation over a 120-day period.

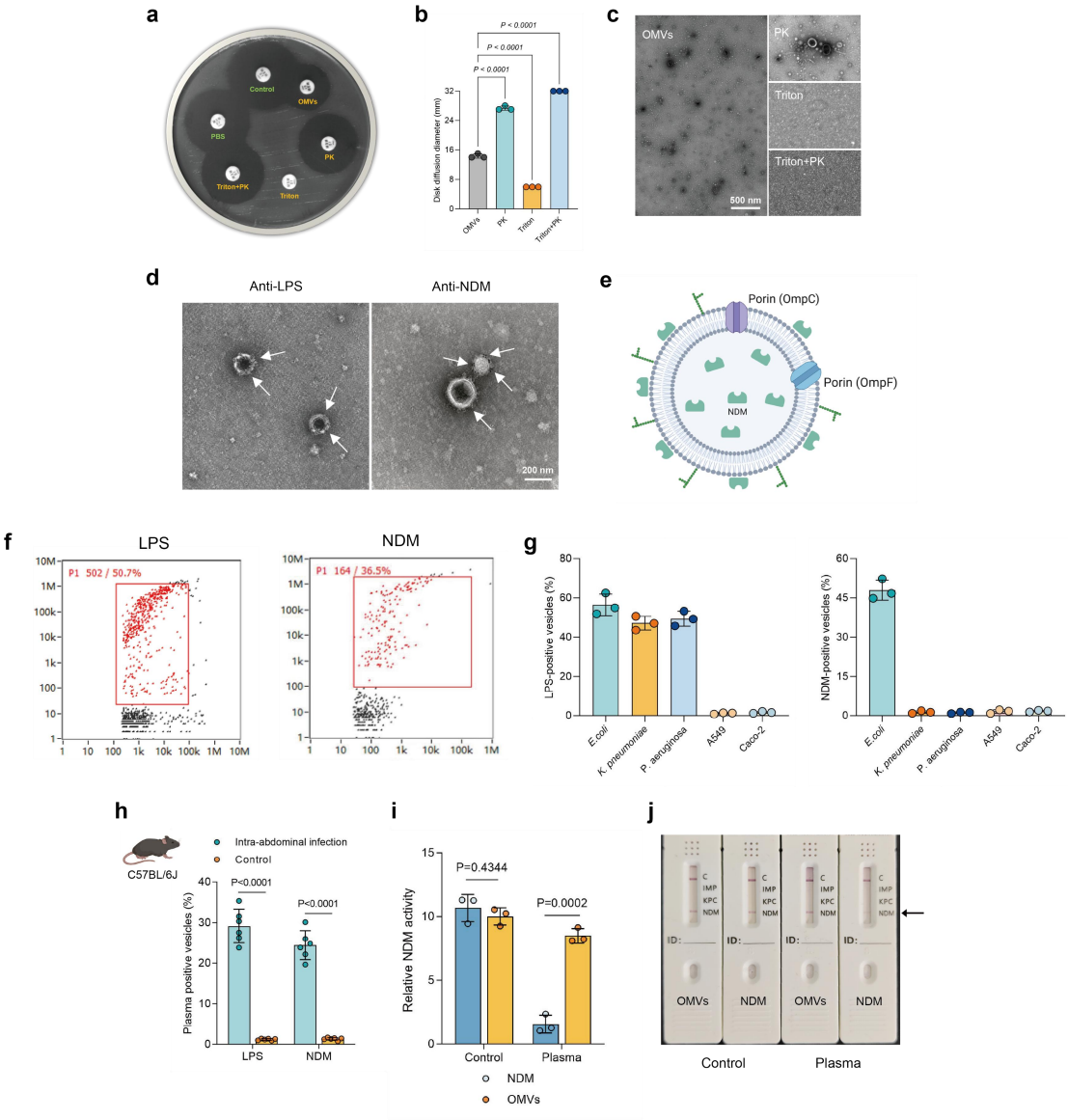


Extended Data Fig. 3. Infecting isolates from persistent and non-persistent infections display similar *in vitro* antimicrobial susceptibility. **a**, **b**, Minimum inhibitory concentration (MIC) distributions of meropenem, ceftazidime, amikacin, and levofloxacin for clinical *Klebsiella pneumoniae* (a) and *Escherichia coli* (b) isolates recovered from persistent and control (non-persistent) infections. **c**, **e**, Bacterial viability of *K. pneumoniae* (c) and *E. coli* (e) isolates from both clinical groups measured before (0 h) and after (4 h) meropenem treatment. **d**, **f**, The corresponding reduction in bacterial burden ($\Delta\log_{10}$CFU/ml) for *K. pneumoniae* (d) and *E. coli* (f) following the 4-hour meropenem exposure. Data points represent independent clinical isolates. Error bars show the standard deviation (SD). Statistical significance was determined using paired (**c**, **e**) or unpaired two-tailed t-tests (**d**, **f**).



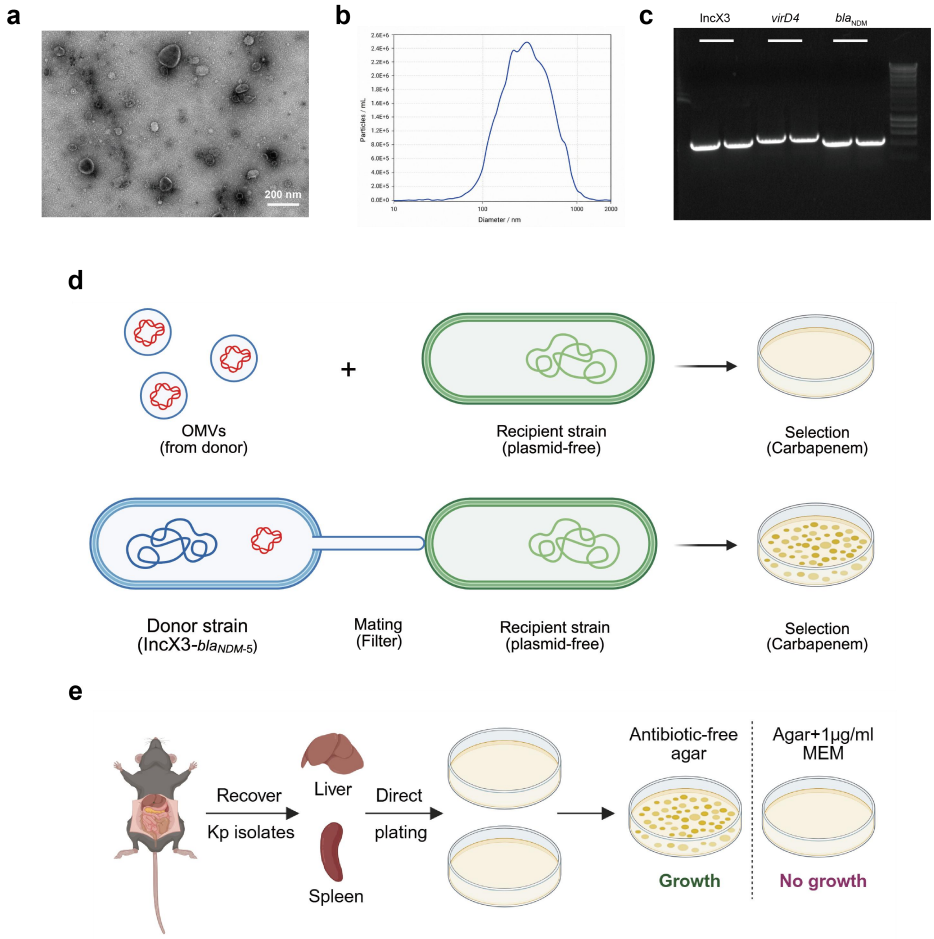
Extended Data Fig. 4. NDM is released into the extracellular environment exclusively via outer membrane vesicles. **a**, Schematic of the clinical screening workflow used to identify fecal CREC colonization from patient rectal swabs, incorporating MacConkey agar with meropenem disks, MALDI-TOF mass spectrometry for strain identification, and broth microdilution for antimicrobial susceptibility testing. **b**, Representative MacConkey agar plates from the screening process, showing fecal CREC colonies growing adjacent to 10-μg meropenem disks. **c**, Schematic detailing the cloning, expression, and purification of recombinant NDM-5 using an *E. coli* BL21 (DE3) expression system. **d**, SDS-PAGE analysis confirming the successful isolation and purity of the recombinant NDM-5 protein. **e**, Colloidal gold immunochromatographic assay detecting NDM in clinical CREC cultures, purified NDM-5, and isolated outer membrane vesicles (OMVs). **f**, Western blot analysis of NDM protein across CREC subcellular fractions. Culture supernatants

were separated by ultrafiltration into 10-100 kDa and >100 kDa fractions; the >100 kDa fraction was further separated by ultracentrifugation into vesicle pellet and pellet-depleted fractions. **g**, Schematic of NDM-mediated meropenem hydrolysis, illustrating the enzymatic cleavage and opening of the β-lactam ring. **h**, Relative NDM carbapenemase activity across subcellular fractions from five dominant CREC sequence types (ST38, ST117, ST131, ST354, and ST405). Enzymatic activity partitions strictly with the >100 kDa fractions, vesicle pellets, and purified OMVs, demonstrating that OMV-dependent NDM secretion is conserved across diverse lineages. Error bars represent the standard deviation (SD).



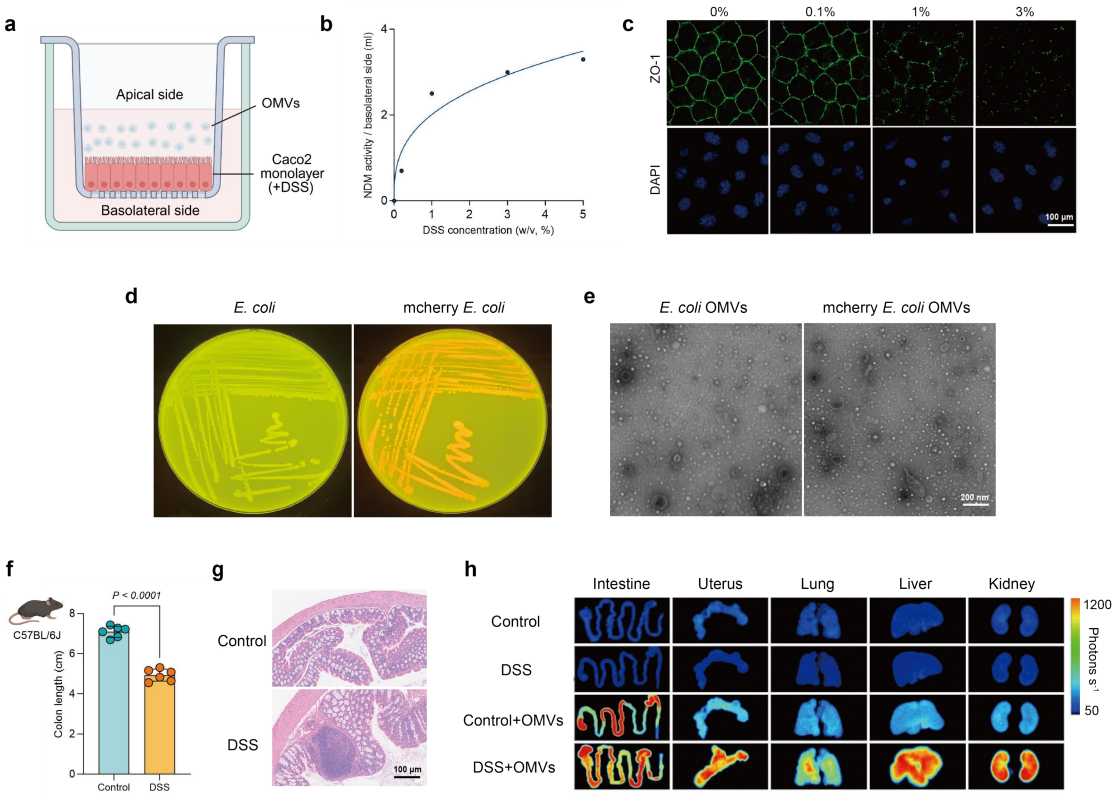
Extended Data Fig. 5. NDM localizes to both the lumen and surface of OMVs and resists plasma-mediated degradation. **a**, **b**, Meropenem disk diffusion assay plate (a) and quantified inhibition zone diameters (b) for meropenem incubated with intact OMVs, OMVs treated with proteinase K (PK), Triton X-100, or a combination of Triton and PK. Proteinase K was used to eliminate surface-exposed NDM. The carbapenem-susceptible *E. coli* MG1655 strain was used as the indicator. **c**, Transmission electron microscopy (TEM) images of the OMVs under the corresponding chemical and enzymatic treatments. Scale bar, 500 nm. **d**, Immunogold

electron microscopy of CREC-derived OMVs using an anti-NDM primary antibody, confirming the surface exposure of NDM (white arrows). Scale bar, 200 nm. **e**, Schematic illustrating the dual localization of NDM within the vesicle lumen and anchored to the outer membrane surface. **f**, **g**, Representative nano-flow cytometry dot plots (f) and quantification (g) of LPS- and NDM-positive extracellular vesicles derived from various bacterial and mammalian cell lines, validating the specificity of the single-vesicle assay. **h**, Percentage of circulating LPS-positive and NDM-positive extracellular vesicles detected in the plasma of mice with an intraperitoneal CREC intra-abdominal infection compared to uninfected controls. **i**, Relative NDM carbapenemase activity of purified free NDM and NDM-loaded OMVs following ex vivo incubation in control buffer versus mouse plasma. Free NDM-5 rapidly lost hydrolytic activity in plasma, whereas OMV-associated NDM-5 remained remarkably stable and active. **j**, Colloidal gold immunochromatographic assay detecting the structural stability of NDM in OMVs versus free NDM after plasma incubation. Error bars represent the standard deviation (SD). Statistical significance was determined using one-way ANOVA with appropriate post-tests (**b**) or unpaired two-tailed t-tests (**h**, **i**).



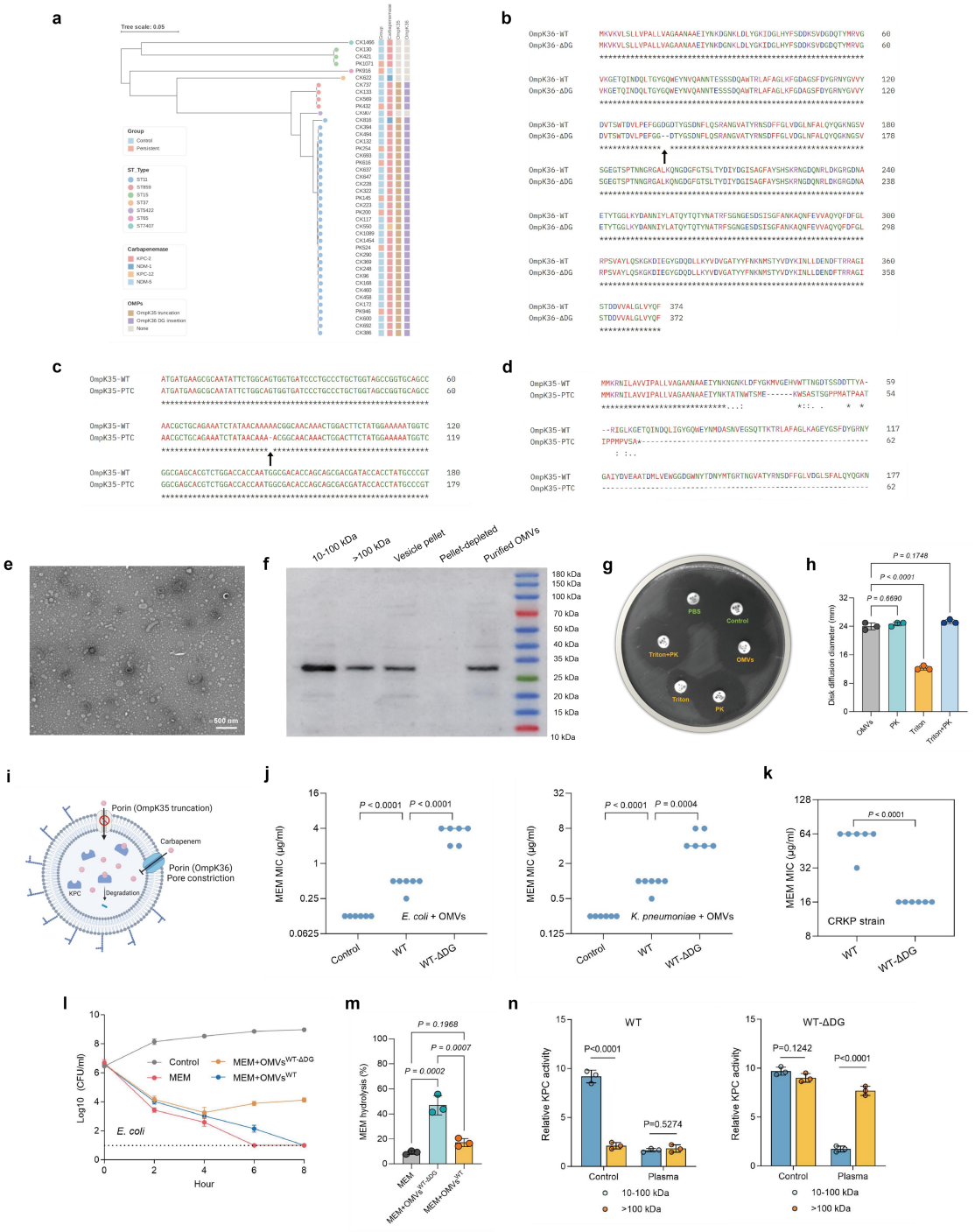
Extended Data Fig. 6. OMVs protect susceptible pathogens without transferring genetic resistance. **a**, Transmission electron microscopy image of the purified OMVs used for the transformation assays. Scale bar, 200 nm. **b**, Size distribution profile of the purified OMVs, measured by nanoparticle tracking analysis. **c**, PCR amplification confirming the presence of the IncX3 plasmid replicon, virD4, and the *bla*$_{\text{NDM}}$ carbapenemase gene within the purified OMVs. **d**, Schematic comparing *in vitro* OMVs-mediated transformation to standard bacterial conjugation. While standard conjugation readily transferred carbapenem resistance to a plasmid-free recipient strain, incubating the recipient with NDM-loaded OMVs failed to produce meropenem-resistant transformants. **e**, *In vivo* confirmation of phenotypic

susceptibility. Infecting *K. pneumoniae* (Kp) isolates recovered from the liver and spleen of mice treated with meropenem plus OMVs grew successfully on antibiotic-free agar but failed to grow on agar supplemented with 1 μg/ml meropenem (MEM). This confirms the surviving bacteria did not acquire genetic resistance during the *in vivo* infection.



Extended Data Fig. 7. Epithelial barrier injury promotes the paracellular translocation and extraintestinal dissemination of gut-derived OMVs. **a**, Schematic of the Caco-2 Transwell assay used to evaluate OMV translocation across an epithelial monolayer following exposure to dextran sulfate sodium (DSS). **b**, NDM carbapenemase activity detected in the basolateral compartment following the application of OMVs and increasing concentrations of DSS (0 to 5% w/v) to the apical side. **c**, Representative immunofluorescence images of Caco-2 monolayers stained for the tight junction protein ZO-1 (green) and nuclei (DAPI, blue) after exposure to the corresponding DSS concentrations. Scale bar, 100 µm. **d**, Agar plate cultures of the CREC reporter strain expressing the OmpF-mCherry fusion protein, visualized under fluorescence. **e**, Transmission electron microscopy images of the purified mCherry-labeled OMVs. Scale bar, 200 nm. **f**, Colon lengths of mice

administered regular drinking water (Control) or 3% DSS to induce mucosal injury. **g**, Representative hematoxylin and eosin (H&E)-stained colon sections confirming DSS-induced structural tissue damage. Scale bar, 100 μm. **h**, Ex vivo optical imaging tracking mCherry fluorescence in the small intestine, ovaries, lungs, liver, and kidneys to evaluate the systemic dissemination of orally administered OMVs. Rows represent mice from the respective control and DSS-treated groups with or without OMVs administration. Plotted data points represent individual mice, with error bars showing the standard deviation (SD). Statistical significance was determined using an unpaired two-tailed t-test (**f**).



Extended Data Fig. 8. Enzyme localization and porin architecture jointly dictate the protective activity of CRKP OMVs. **a**, Core-genome phylogenetic tree of fecal colonized carbapenem-resistant *K. pneumoniae* (CRKP) isolates from the cohort. Annotations display the sequence type (ST), carbapenemase type (predominantly KPC-2), and outer membrane porin (OMP) mutations. **b-d**, Sequence alignments

highlighting the Asp-Gly (DG) insertion in the OmpK36 channel (b) and the frameshift mutation causing OmpK35 truncation (c, d) in the dominant ST11 clone. PTC, premature terminal codon. **e**, Transmission electron microscopy image of purified OMVs derived from the ST11 CRKP strain. Scale bar, 500 nm. **f**, Western blot analysis of KPC protein across ST11 CRKP subcellular fractions. Culture supernatants were separated by ultrafiltration into 10-100 kDa and >100 kDa fractions; the >100 kDa fraction was further separated by ultracentrifugation into vesicle pellet and pellet-depleted fractions. **g**, **h**, Meropenem disk diffusion assay plate (g) and quantified inhibition zone diameters (h) for meropenem incubated with intact OMVs, OMVs treated with proteinase K (PK), Triton X-100, or a combination of Triton and PK. The carbapenem-susceptible *E. coli* MG1655 strain was used as the indicator. The data demonstrate that functional KPC-2 is confined within the OMV lumen and protected from surface degradation. **i**, Schematic illustrating OmpK35 truncation and OmpK36 pore constriction restrict carbapenem entry into the OMVs lumen, preventing KPC-mediated degradation. **j**, Meropenem MICs for susceptible *E. coli* (left) and *K. pneumoniae* (right) incubated with OMVs derived from the wild-type ST11 parent (WT) or the isogenic OmpK36-revertant lacking the DG insertion (WT-ΔDG). **k**, Meropenem MICs for the parent CRKP strain (WT) versus the WT-ΔDG revertant. **l**, Time-kill curves for carbapenem-susceptible *E. coli* treated with meropenem (MEM) alone or combined with OMVs from the WT or WT-ΔDG ST11 CRKP strains. **m**, Percentage of meropenem hydrolysis measured during the time-kill assay. **n**, Relative KPC carbapenemase activity of free (10-100 kDa) and

OMVs-associated (>100 kDa) fractions from WT and WT-ΔDG ST11 CRKP strains following ex vivo incubation in control buffer versus mouse plasma. Error bars represent the standard deviation (SD). Statistical significance was determined using one-way ANOVA with appropriate post-tests (**h**, **j**, **m**) or unpaired two-tailed t-tests (**k**, **n**).